ACS Combinatorial Science

Research Article

pubs.acs.org/acscombsci

Doped SnO_2 Transparent Conductive Multilayer Thin Films Explored by Continuous Composition Spread

Jin Ju Lee,[†,‡] Jong-Yoon Ha,[§] Won-Kook Choi,[∥] Yong Soo Cho,[‡] and Ji-Won Choi*[,†,ϕ]

[†]Electronic Materials Research Center, Korea Institute of Science and Technology, Seoul 136-791, Republic of Korea

[‡]Department of Materials Science and Engineering, Yonsei University, Seoul 120-749, Republic of Korea

[§]Institute for Research in Electronics and Applied Physics, University of Maryland, College Park Maryland 20742, United States

[∥]Interface Control Research Center, Korea Institute of Science and Technology, Seoul 136-791, Republic of Korea

[ϕ]Department of Nanomaterials Science and Technology, Korea University of Science and Technology, Daejeon 305-333, Republic of Korea

ABSTRACT: Mn-doped SnO_2 thin films were fabricated by a continuous composition spread (CCS) method on a glass substrate at room temperature to find optimized compositions. The fabricated materials were found to have a lower resistivity than pure SnO_2 thin films because of oxygen vacancies generated by Mn doping. As Mn content was increased, resistivity was found to decrease for limited doping concentrations. The minimum thin film resistivity was 0.29 Ω-cm for a composition of 2.59 wt % Mn-doped SnO_2. The Sn−O vibrational stretching frequency in FT-IR showed a blue shift, consistent with oxygen deficiency. Mn-doped SnO_2/Ag/Mn-doped SnO_2 multilayer structures were fabricated using this optimized composition deposited by an on-axis radio frequency (RF) sputter. The multilayer transparent conducting oxide film had a resistivity of 7.35×10^{-5} Ω-cm and an average transmittance above 86% in the 550 nm wavelength region.

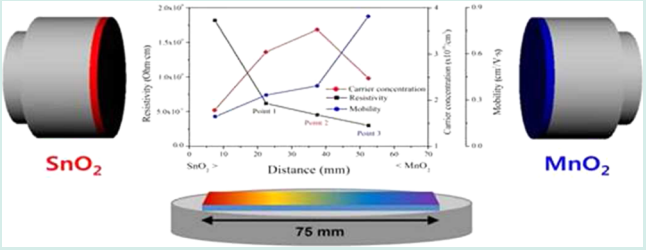

KEYWORDS: *Mn-SnO_2, multilayer, continuous composition spread, transparent conducting oxide*

INTRODUCTION

Most optically transparent and electrically conducting oxides (TCOs) are binary or ternary compounds, containing one or two metallic elements. Tin-doped In_2O_3 (ITO), Al-doped ZnO, and antimony- or fluorine-doped SnO_2 are used as TCO materials for many applications including display devices,[1] thin film transistors,[2] gas sensors,[3] infrared reflection glasses, and solar cells.[4] In particular, ITO is used extensively because of its low resistivity ($<10^{-4}$ Ω-cm) and high transmittance (>80%) in the visible region.[5] However, the scarcity and high price of indium have created a need for its replacement in the rapidly developing display industry.

SnO_2- and ZnO-based TCO thin films have emerged as strong alternatives to ITO films because Sn and Zn are found in high abundance, are nontoxic or only moderately toxic in oxide form, and have good thermal stability. Although indium-free TCO materials, including Al-doped ZnO,[6] Ga-doped ZnO,[7] and F-doped SnO_2,[8] have higher transmittances, their resistivities are still higher than that of ITO. To obtain high quality TCOs, high temperature annealing is typically required. As part of the considerable effort to avoid such processes for TCO materials, multilayer oxide/metal/oxide (OMO) materials have been suggested to overcome the limits of both electrical resistivity and optical transmittance of single-layer TCOs at low temperature.[9] It is reported that dielectric/metal/dielectric multilayer structures can increase both transparency in the visible wavelength range (because of the antireflection properties of successive layers having different refractive indices) and conductivity (through carrier injection because of differences in work functions at interfaces between metal and transparent semiconducting oxides).[9] The smoothness of the oxide film surface is an important factor in multilayer OMO

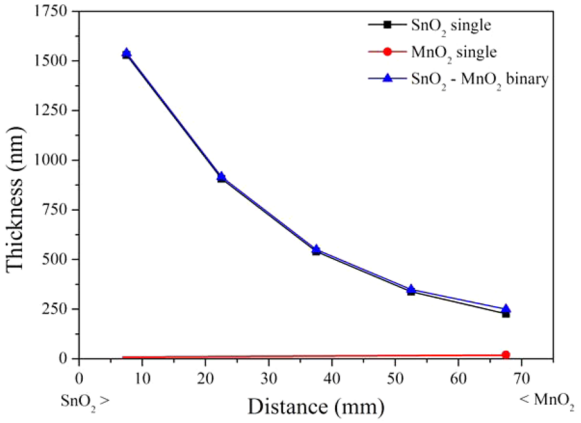

Figure 1. Thickness profile of SnO_2−MnO_2 thin films deposited at room temperature on a glass substrate by off-axis RF sputtering-CCS.

Received: December 16, 2014
Revised: March 9, 2015
Published: March 11, 2015

DOI: 10.1021/co500185d
ACS Comb. Sci. 2015, 17, 247−252

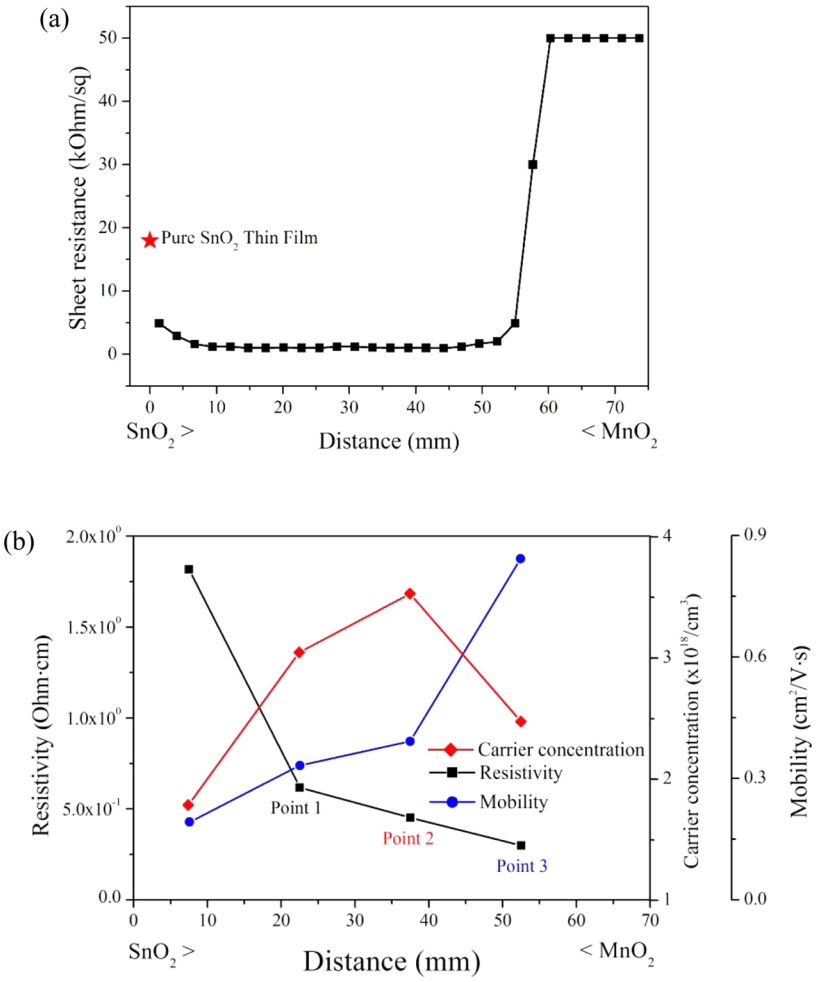

Figure 2. Electrical properties of Mn-doped SnO_2 thin films deposited at room temperature (a) sheet resistance (b) resistivity, mobility, and carrier concentration.

structures because of the use of ultrathin metal films between oxide layers and so, an amorphous oxide film is preferred.

SnO_2-based TCO materials maintain an amorphous phase below their crystallization temperature of 400 °C with excellent acid resistance, low cost, air stability, good transparency, and chemical stability. Even though SnO_2-based materials, such as F-doped SnO_2,[8] Sb-doped SnO_2,[10] and Ta-doped SnO_2,[11] have poorer electrical properties than ITO, these properties can be sufficient in the OMO structure. A few papers have appeared on the electrical and optical properties of Mn-doped SnO_2 thin films, describing the complexity of the valence state of the Mn ion.[12,13] Manganese ions can be incorporated into the lattice in the form of Mn^{3+} (65 pm radius) or Mn^{4+} (54 pm radius), since both ionic radii are smaller than that of Sn^{4+} (69 pm). Therefore, the electrical, optical, and dilute magnetic properties of Mn-doped SnO_2 thin films are expected to be interesting due to the multivalence of the films.

$Sn_{1-x}Mn_xO_2$ semiconductor materials[14,15] were selected here because they exhibit useful semiconductor and optical properties and the SnO_2 material is a strong alternative to ITO. The full range of Mn-doped SnO_2 TCOs was deposited to find an optimized composition for a multilayer OMO structure by a continuous composition spread (CCS) at room temperature. CCS is a well-known method for the discovery and optimization of new material systems on a substrate with binary or ternary compositions.[7] The electrical, optical, and physical properties of the gradient materials were evaluated, and the multilayer OMO structure TCO was found to be realized by the optimized Mn-doped SnO_2 composition produced in the CCS method.

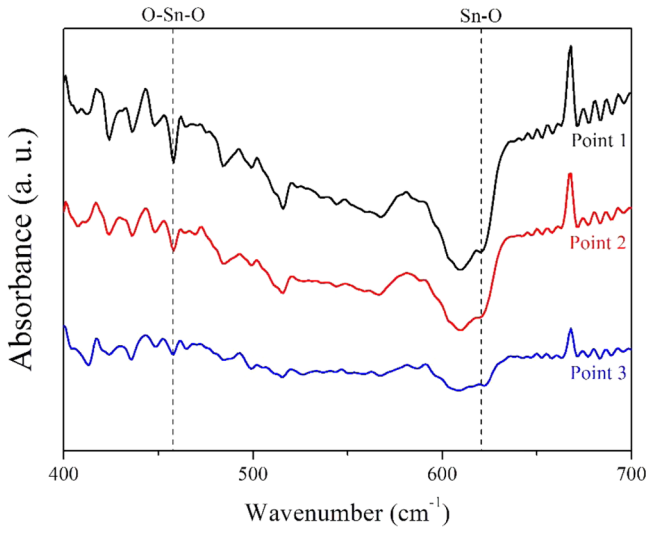

Figure 3. FT-IR spectra of Mn-doped SnO_2 thin films deposited at room temperature.

DOI: 10.1021/co500185d
ACS Comb. Sci. 2015, 17, 247−252

RESULTS AND DISCUSSION

Figure 1 shows the thickness profiles of SnO_2−MnO_2 binary, SnO_2, and MnO_2 thin films by an off-axis RF sputtering-CCS system at room temperature. The thicknesses of each film were measured by cross-sectional scanning electron microscopy (SEM). Compositions and deposition rates of the thin films were changed depending on distances from SnO_2 and MnO_2 targets in the CCS system. As the distance from the target was increased, the deposition rates decreased as shown in Figure 1. The thickness profiles of the SnO_2 thin film show overlap with the binary SnO_2−MnO_2 thin film because of the small thickness of MnO_2 thin film in the SnO_2−MnO_2 binary.

The electrical properties of Mn-doped SnO_2 thin films deposited at room temperature on a glass substrate are shown in Figure 2. The resistivity of the films decreased with increased Mn content. Extremely low-level Mn doping concentrations were utilized because high level Mn doped SnO_2 thin films show higher resistivity than pure SnO_2 thin films. With film deposition, we expected that Mn ions were inclined to incorporate into the lattice in the form of Mn^{3+} (65 pm radius) ions or Mn^{4+} (54 pm radius) since both ionic radii are smaller that of Sn^{4+} (69 pm). The effect of the Mn^{3+} ions in the film is discussed later on in the manuscript. On the basis of the above rational, the generated Mn^{3+} ions in the film affect film electrical properties. The minimum value of resistivity for the film was determined to be 0.29 Ω-cm (point 3 in Figure 2b).

Figure 3 demonstrates the FT-IR spectra of Mn-doped SnO_2 at 400−700 cm^{-1} to detect a defects in the films.[16] Three points in the low resistivity region were selected (Figure 2b). The main IR features of SnO_2 at 458 and 620 cm^{-1} are assigned to O−Sn−O and Sn−O stretching bond vibrations,[17,18] respectively. It was found that the Sn−O stretching vibration frequency showed a blue shift from 620 to 622 cm^{-1} when Mn content was increases from point 1 to point 3. Oxygen deficiency with the increment of Mn contents resulted in the blue shift. A number of oxygen vacancies (V_O) are produced through substitutional doping of Mn^{3+} for Sn^{4+} to maintain charge balance. Therefore, the increase of Mn concentration promotes the increase of V_O defects resulting in blue shift.[19] This blue shift could explain why the resistivity of the Mn-doped SnO_2 films decreases with increasing Mn concentration.

The experimental XANES recorded at both the Sn L_2-edge and Mn K-edge in the Mn-doped SnO_2 films are shown in Figure 4. Figure 4a shows the Sn L_2-edge XANES of Mn-doped SnO_2 thin films deposited by CCS. The spectral features of each film were similar and are in agreement with calculated values.[20] Figure 4b shows the Mn K-edge XANES. As Mn content was increased, from point 1 to point 3, the relative intensity of the Mn^{2+}/Mn^{4+} K-edge increased. This result suggested that the average valence state of manganese decreased with Mn doping from Mn^{4+} toward Mn^{3+}.[21] The XANES spectra are in well agreement with the FT-IR data.

The structural properties of Mn-doped SnO_2 films were examined by XRD as shown in Figure 5(a). The thin films at point 1, 2, and 3 showed amorphous structures due to the high crystallization temperature of SnO_2. In addition, a broad band of weak diffractions were observed, and no diffraction peaks corresponding to Mn oxides, such as MnO, Mn_2O_3, and MnO_2, or any Sn/Mn ternary oxides were detected. Figure 5b shows the atomic force microscopy (AFM) topological surface images of the films. The scanning area of the AFM measurement was 20 × 20 μm^2. Surface root-mean-square (RMS) values of the

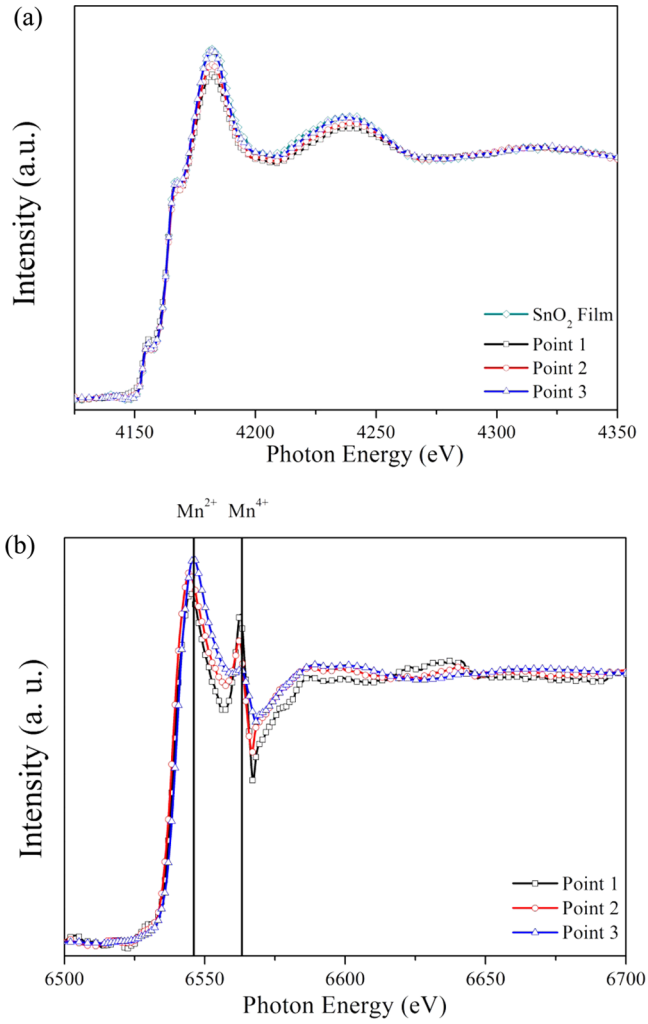

Figure 4. XANES of Mn-doped SnO_2 thin films deposited at room temperature as a function of point (a) Sn L_2-edge and (b) Mn K-edge.

films from point 1 to 3 were determined to be 0.8, 0.6, and 0.8 nm, respectively. These films presented very smooth surfaces which can be used to deposit a uniform Ag metal layer in multilayer oxide/metal/oxide (OMO) structures. The low RMS of the films can help to improve transmittance, because scattering of defects is suppressed by the smooth surface.

To evaluate composition in elemental ratios across the sample, 2 MeV $4He^{+2}$ backscattering spectroscopy (BS) measurements were carried out. The backscattering spectrum was simulated by a RUMP code to obtain the concentration (atomic %) at point 3. The experimental backscattering spectrum and calculated concentration at point 3 is shown in Figure 6. The composition of point 3 is $Sn_1Mn_{0.045}O_{2.35}$ and corresponds to 2.59 wt % Mn-doped SnO_2.

A 2.59 wt % Mn-doped SnO_2 composition was developed by the CCS method. A OMO structure using the composition was then realized by on-axis RF and DC sputtering systems. Each layer, Mn-doped SnO_2/Ag/Mn-doped SnO_2, was deposited to 50, 12, and 50 nm thick, respectively. To compare the properties of the OMO structures, three different compositions of 0, 2.59, and 10 wt % Mn-doped SnO_2 layers were prepared. Figure 7 shows the electrical properties of Mn-doped SnO_2/Ag/Mn-doped SnO_2 thin film multilayers deposited at room temperature with various Mn contents. The lowest resistivity and sheet resistance of the multilayer films was determined to

DOI: 10.1021/co500185d
ACS Comb. Sci. 2015, 17, 247−252

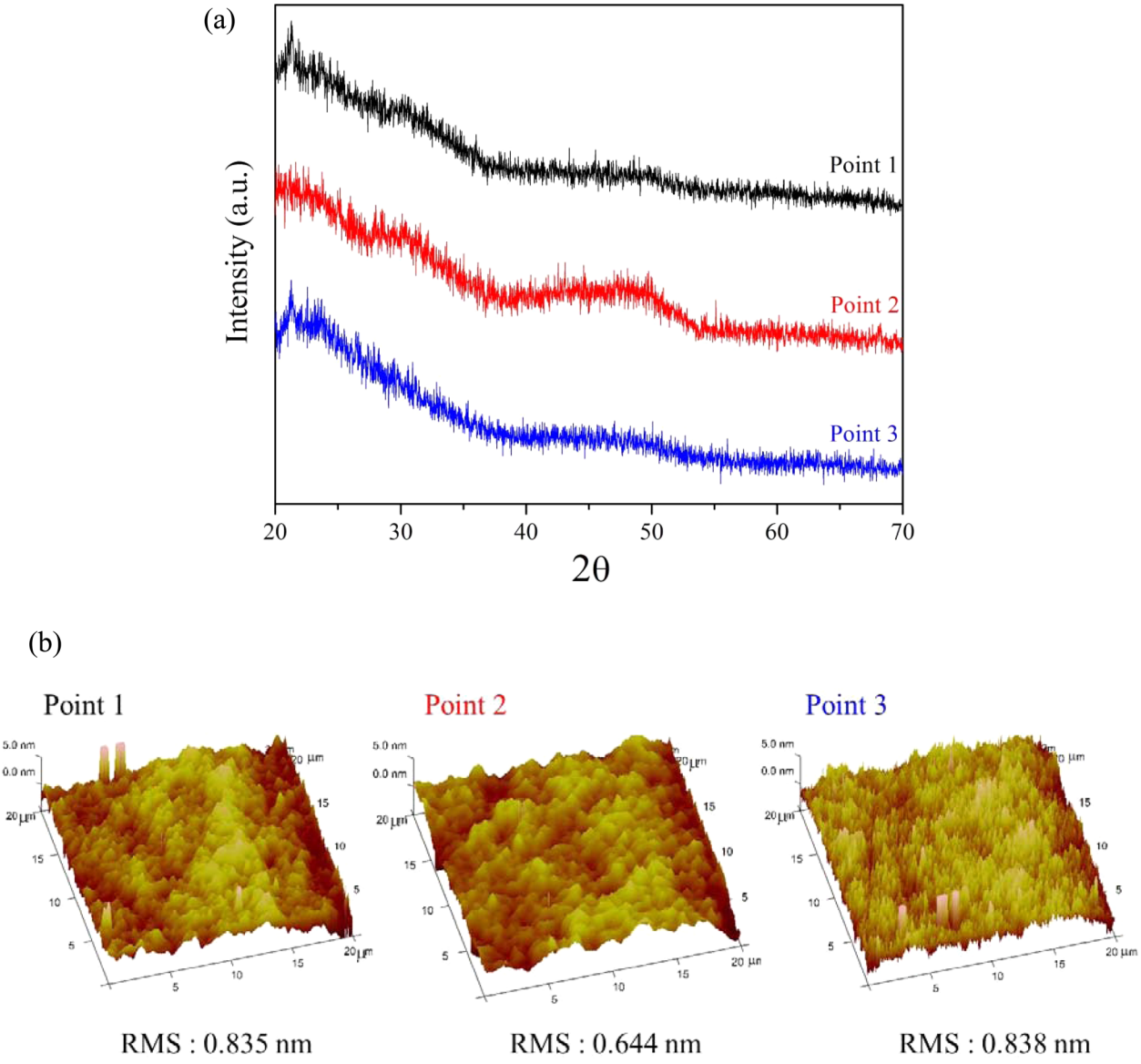

Figure 5. (a) X-ray diffraction patterns and (b) AFM images of Mn-doped SnO_2 thin films deposited at room temperature.

be 7.35 × 10^{-5} Ω-cm and 6.57 Ohm/sq at 2.59 wt % Mn content, respectively. Resistivity and sheet resistance of OMO structures decreased and then dramatically increased with increased Mn content. These results agree with the electrical properties of the single Mn-doped SnO_2 layer shown in Figure 2. In addition, OMO structures demonstrate improved electrical properties compared to the pure SnO_2 layer.

The optical transmittance of the multilayered thin film deposited with various Mn contents at room temperature was investigated in the 200−900 nm wavelength region. Figure 8 shows the optical transmittance of the OMO multilayer films from 0 to 10 wt % of Mn. Typically, the optical transmittance of display products requires a standard wavelength of 550 nm because the human eye is most sensitive to 550 nm. The transmittance of each sample (0, 2.59, and 10 wt % Mn) has 82%, 86%, and 81% at 550 nm, respectively. Our optimized transparent conducting material, 2.59 wt % Mn-doped SnO_2, in the OMO structure was very promising because it had ideal electrical and optical properties even though it was deposited at room temperature without any heat treatment process.

CONCLUSIONS

Binary SnO_2−MnO_2 thin films were fabricated by continuous composition spread (CCS) method on a glass substrate at room temperature to determine optimized compositions. The resistivity of Mn-doped SnO_2 thin films decreased with increasing Mn content, subsequently generating oxygen vacancies. The minimum resistivity of the thin film was 0.29 Ω-cm. In addition, blue shift of the Sn−O stretching vibration frequency in FT-IR was interpreted as the effect of oxygen deficiency. As Mn content increased, the peak of the Mn K-edge was slightly decreased indicating that the average valence state of manganese changed from Mn^{4+} to Mn^{3+}. The transmittances of the films having good electrical properties showed about 80% in the 550−900 nm wavelength region. RBS analysis determined 2.59 wt % Mn-doped SnO_2 as the optimized composition. Multilayer 2.59 wt % Mn-doped SnO_2/Ag/2.59 wt % Mn-doped SnO_2 structure was fabricated by an on-axis RF and DC sputtering method. This structure had a resistivity of 7.35 × 10^{-5} Ω-cm and a transmittance above 86% at 550 nm. The OMO structures including Mn-doped SnO_2 layers and an Ag layer

DOI: 10.1021/co500185d
ACS Comb. Sci. 2015, 17, 247−252

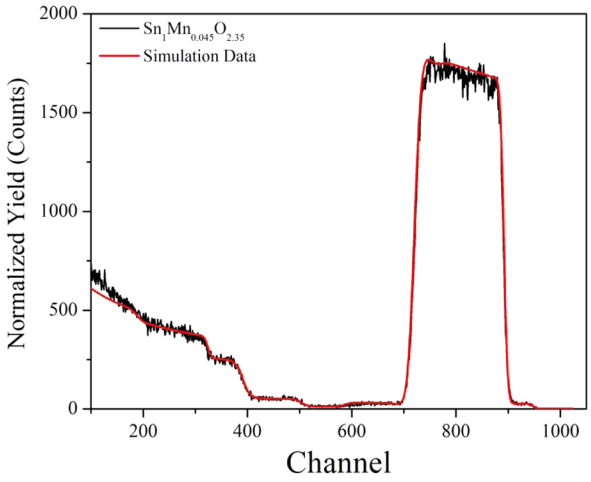

Figure 6. RBS compositional analysis at the point 3 of the Mn-doped SnO_2 thin film.

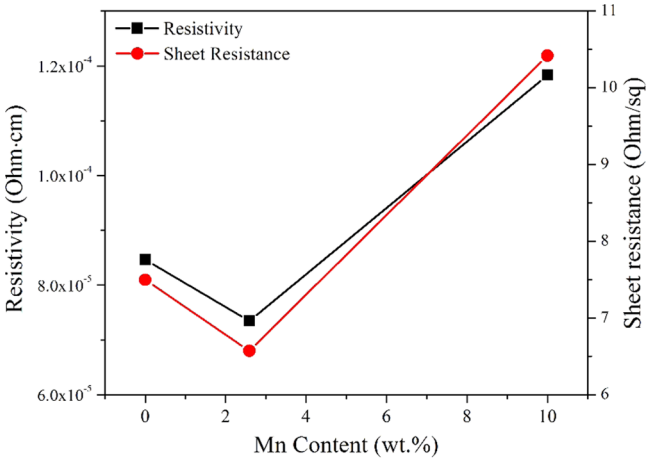

Figure 7. Resistivity and sheet resistance of Mn-doped SnO_2/Ag/Mn-doped SnO_2 thin film multilayers deposited at room temperature as a function of Mn content.

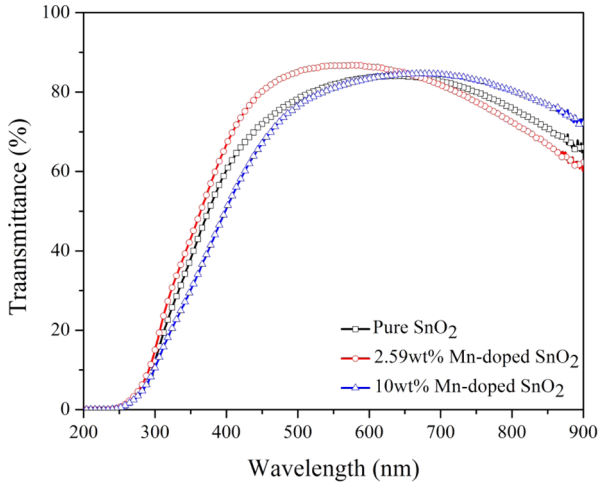

Figure 8. Optical transmittance of Mn-doped SnO_2/Ag/Mn-doped SnO_2 thin film multilayers deposited at room temperature as a function of the Mn content.

deposited at room temperature show both good electrical and optical properties.

EXPERIMENTAL PROCEDURES

Mn-doped SnO_2 thin films were prepared by an off-axis RF sputtering-CCS system on a glass substrate (75 mm × 15 mm) at room temperature. Figure 9 shows a schematic of the CCS. A

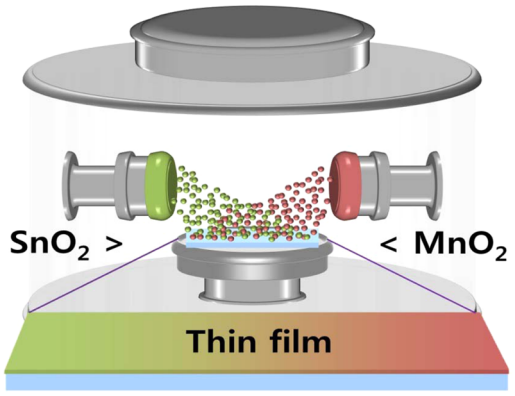

Figure 9. Schematic of the off-axis RF sputtering−CCS system.

tin oxide (SnO_2) target (2 in., 99.99%, CERAC) and a manganese oxide (MnO_2) target (2 in., 99.99%, CERAC) were used to explore the optimized compositions of Mn-doped SnO_2. The base pressure of the sputtering chamber was kept at 2.7×10^{-4} Pa. The sputtering was carried out with 6 Pa of argon for 1 h. The MnO_2 and SnO_2 targets were powered by independent RF supplies (MnO_2, 10 W; SnO_2, 40 W) to achieve the desired composition range on the substrate.

Three different targets, 0, 2.59, and 10 wt % Mn-doped SnO_2, were fabricated by the conventional solid-state method. The Mn-doped SnO_2/Ag/Mn-doped SnO_2 multilayer structure was demonstrated by on-axis RF and DC sputtering systems at room temperature. Each layer of Mn-doped SnO_2 was deposited to 50, 12, and 50 nm thick, respectively. The RF and DC sputtering were carried out with 6 and 0.66 Pa of argon, respectively.

Thicknesses of the thin films were examined through cross-sectional observation by SEM (XL-30 FEG). Electrical properties of the films including sheet resistance, carrier concentration, and mobility, were measured using a four-point probe method (MCP-T600, Mitsubishi Chemical) and Hall measurement system. The films were analyzed in the 400−700 wavenumber range by FT-IR spectroscopy (Frontier, PerkinElmer). Electronic states were studied using X-ray absorption near edge structure (XANES, ID KIST-PAL). The structural properties and surface roughness of the films were investigated by X-ray diffraction (XRD, Rigaku) and atomic force microscopy (AFM, Veeco), respectively. The optical properties were measured using UV−vis spectrometry (Lambda 18, PerkinElmer) in the range of 200−900 nm. The optimized composition of manganese tin oxide thin films was characterized by RBS (6SDH2, NEC).

AUTHOR INFORMATION

Corresponding Author

*E-mail: jwchoi@kist.re.kr. Tel: +82-2-958-5556. Fax: +82-2-958-6720.

Author Contributions

J.J.L. performed film deposition and dielectric measurements. J.-W.C. supervised the experiments and contributed to manuscript preparation. J.J.L., J.-Y.H., W.-K.C., Y.S.C., and J.-W.C.

DOI: 10.1021/co500185d
ACS Comb. Sci. 2015, 17, 247−252

analyzed the data and wrote the manuscript. J.-W.C. conceived the idea and initiated and directed the research. All authors discussed the progress of research and reviewed the manuscript. The manuscript was written through contributions of all authors. All authors have given approval to the final version of the manuscript.

Funding

This study was supported by the ATC program (No. 10048659) and the Core Technology of Materials Research and Development Program (No. 10041232) funded by the Ministry of Trade, Industry & Energy, and also partially by the K-GRL(2Z04060) and the KIST Future Resource Program-(2E24770).

Notes

The authors declare no competing financial interest.

REFERENCES

(1) Alam, M. J.; Cameron, D. C. Optical and electrical properties of transparent conductive ITO thin films deposited by sol−gel process. *Thin Solid Films* **2000**, *377*, 455−459.

(2) Ting, C. C.; Chang, S. P.; Li, W. Y.; Wang, C. H. Enhanced performance of indium zinc oxide thin film transistor by yttrium doping. *Appl. Surf. Sci.* **2013**, *284*, 397−404.

(3) Parthibavarman, M.; Renganathan, B.; Sastikumar, D. Development of high sensitivity ethanol gas sensor based on Co-doped SnO_2 nanoparticles by microwave irradiation technique. *Curr. Appl. Phys.* **2013**, *13* (7), 1537−1544.

(4) Kambe, M.; Fukawa, M.; Taneda, N.; Sato, K. Improvement of a-Si solar cell properties by using SnO_2: F TCO films coated with an ultra-thin TiO_2 layer prepared by APCVD. *Sol. Energy Mater. Sol. Cells* **2006**, *90* (18−19), 3014−3020.

(5) Ma, Q. H.; Nathan, A. Room temperature sputter deposition of polycrystalline ITO for photodetectors. *Proc.—Electrochem. Soc.* **1999**, *98* (22), 408−420.

(6) Jung, K.; Shin, D. W.; Yoon, S. J.; Choi, J. W.; Choi, W. K.; Song, J. H.; Kim, H. J. Electrical and optical properties of Al-doped zinc-oxide thin films deposited at room temperature by using the continuous composition spread method. *J. Korean Phys. Soc.* **2010**, *57* (4), 1092−1095.

(7) Jung, K.; Choi, W. K.; Yoon, S. J.; Kim, H. J.; Choi, J. W. Influence of substrate temperature on the electrical and optical properties of Ga-doped ZnO thin films fabricated by continuous composition spread. *Ceram. Int.* **2012**, *38*, S605−S608.

(8) Gao, K. H.; Lin, T.; Liu, X. D.; Zhang, X. H.; Li, X. N.; Wu, J.; Liu, Y. F.; Wang, X. F.; Chen, Y. W.; Ni, B.; Dai, N.; Chu, J. H. Low temperature electrical transport properties of F-doped SnO_2 films. *Solid State Commun.* **2013**, *157*, 49−53.

(9) Yang, J. D.; Cho, S. H.; Hong, T. W.; Son, D. I.; Park, D. H.; Yoo, K. H.; Choi, W. K. Organic photovoltaic cells fabricated on a SnO_x/Ag/SnO_x multilayer transparent conducting electrode. *Thin Solid Films* **2012**, *520*, 6215−6220.

(10) Yang, W. H.; Yu, S. H.; Zhang, Y.; Zhang, W. F. Properties of Sb-doped SnO_2 transparent conductive thin films deposited by radio-frequency magnetron sputtering. *Thin Solid Films* **2013**, *542*, 285−288.

(11) Muto, Y.; Nakatomi, S.; Oka, N.; Iwabuchi, Y.; Kotsubo, H.; Shigesato, Y. High-rate deposition of Ta-doped SnO_2 films by reactive magnetron sputtering using a Sn−Ta metal-sintered target. *Thin Solid Films* **2012**, *520* (10), 3746−3750.

(12) Brahma, R.; Krishna, M.; Bhatnagar, A. Optical, structural and electrical properties of Mn doped tin oxide thin films. *Bull. Mater. Sci.* **2006**, *29* (3), 317−322.

(13) Lee, C.; Pandey, R.; Wang, B.; Choi, W.; Choi, D.; Oh, Y. Nano-sized indium-free MTO/Ag/MTO transparent conducting electrode prepared by RF sputtering at room temperature for organic photovoltaic cells. *Sol. Energy Mater. Sol. Cells* **2015**, *132*, 80−85.

(14) Gao, K. H.; Li, Z. Q.; Liu, X. J.; Song, W.; Liu, H.; Jiang, E. Y. Bulk $Sn_{1-x}Mn_xO_2$ magnetic semiconductors without room-temperature ferromagnetism. *Solid State Commun.* **2006**, *138*, 175−178.

(15) Kimura, H.; Fukumura, T.; Kawasaki, M.; Inaba, K.; Hasegawa, T.; Koinuma, H. Rutile-type oxide-diluted magnetic semiconductor: Mn-doped SnO_2. *Appl. Phys. Lett.* **2002**, *80*, 94−96.

(16) Mazumder, N.; Bharati, A.; Saha, S.; Sen, D.; Chattopadhyay, K. K. Effect of Mg doping on the electrical properties of SnO_2 nanoparticles. *Curr. Appl. Phys.* **2012**, *12* (3), 975−982.

(17) Ungureanu, A.; Anadronescu, C.; Voice, G.; Scoban, A.; Oprea, O.; Stanica, N.; Jitaru, I. Structural characterisation and luminescence properties of paramagnetic Mn doped SnO_2 nanopowders obtained via simple buthanol assisted sol-gel synthesis. *Dig. J. Nanomater. Biostructures (DJNB)* **2013**, *8* (3), 1169−1178.

(18) Zhang, B.; Tian, Y.; Zhang, J.; Cai, W. Structural, optical, electrical properties and FTIR studies of fluorine doped SnO_2 films deposited by spray pyrolysis. *J. Mater. Sci.* **2011**, *46* (6), 1884−1889.

(19) Liu, X.; Iqbal, J.; Wu, Z.; He, B.; Yu, R. Structure and room-temperature ferromagnetism of Zn-doped SnO_2 nanorods prepared by solvothermal method. *J. Phys. Chem. C* **2010**, *114* (11), 4790−4796.

(20) Özkendır, O. M.; Ufuktepe, Y. Electronic and structural properties of SnO and SnO_2 thin films studied by X-ray-absorption spectroscopy. *J. Optoelectronıcs Adv. Mater.* **2007**, *9*, 3729−3733.

(21) Sikora, M.; Kapusta, C.; Knížek, K.; Jirák, Z.; Autret, C.; Borowiec, M.; Oates, C. J.; Procházka, V.; Rybicki, D.; Zajac, D. *XANES Study of* $LaMn_{1-x}Co_xO_3$ *Series*, Hasylab Annual Report: DESY: Hamburg, 2005; pp 713−714.

DOI: 10.1021/co500185d
ACS Comb. Sci. 2015, 17, 247−252